ARTICLES

Classical vs Quantum Vibrational Energy Relaxation Pathways in Solvated Polyatomic Molecules

Being J. Ka and Eitan Geva*

Department of Chemistry, University of Michigan, Ann Arbor, Michigan 48109-1055

Received: June 22, 2006; In Final Form: October 3, 2006

Vibrational energy relaxation (VER) of solvated polyatomic molecules can occur via different pathways. In this paper, we address the question of whether treating VER *classically or quantum-mechanically* can lead to different predictions with regard to the preferred pathway. To this end, we consider the relaxation of the singly excited asymmetric stretch of a rigid, symmetrical, and linear triatomic molecule (A-B-A) in a monatomic liquid. In this case, VER can occur either directly to the ground state or indirectly via intramolecular vibrational relaxation (IVR) to the symmetric stretch. We have calculated the rates of these two different VER pathways via classical mechanics and the linearized semiclassical (LSC) method. When the mass of the terminal A atoms is significantly larger than that of the central B atom, we find that LSC points to intermolecular VER as the preferred pathway, whereas the classical treatment points to IVR. The origin of this trend reversal appears to be purely quantum-mechanical and can be traced back to the significantly weaker quantum enhancement of solvent-assisted IVR in comparison to that of intermolecular VER.

I. Introduction

Vibrational energy relaxation (VER) is the fundamental process by which an excited vibrational mode releases its excess energy to other, intermolecular and/or intramolecular, degrees of freedom (DOF). Virtually all chemical phenomena in the condensed phase involve VER processes. The measurement and calculation of VER rates in such systems have therefore received much attention over the last few decades.[1−79]

In recent experimental studies of VER, attention has been shifting to polyatomic solute/solvent systems.[43−79] The main new feature of VER in polyatomic molecules, as opposed to diatomic molecules, has to do with the fact that it can occur via different intramolecular and/or intermolecular pathways. The case of small polyatomic molecules (3−4 atoms) is particularly attractive because the modes that define the vibrational spectrum are more or less isolated and the number of VER pathways is relatively small.

The wealth of detailed experimental information on VER in polyatomic solute/solvent systems has motivated many theoretical studies that attempted to provide a molecular interpretation of the observed time scales and pathways in such systems.[70−79] Those theoretical studies have been based mostly on the Landau−Teller formula, which puts the VER rate constant in terms of the Fourier transform (FT), evaluated at a frequency corresponding to the energy gap between a pair of vibrational states, of a certain correlation function involving the forces exerted on the solute by the solvent.[27,80] Most previous studies of VER in polyatomic systems implemented this formalism within the framework of classical mechanics. However, replacing the quantum-mechanical force−force correlation function (FFCF) by its classical counterpart is not necessarily justified in cases where the energy gap between the vibrational levels is larger than k_BT. Indeed, discrepancies by many orders of magnitude have been reported between experimentally measured VER rates and predictions based on classical molecular dynamics simulations.[81−86] At the same time, a numerically exact calculation of the quantum-mechanical FFCF in liquid solutions is not feasible. Several previous studies of VER in polyatomic systems have employed quantum correction factors (QCFs) in order to bypass this problem.[70,74,77,87] Unfortunately, the choice of QCF is often rather ad-hoc and estimates obtained from different QCFs can differ by orders of magnitude, particularly when high-frequency vibrations are involved.

We have recently introduced a new approach for calculating VER rate constants, which is based on estimating the quantum-mechanical FFCF via the linearized semiclassical (LSC) approximation. The approximation involves linearizing the forward−backward path-integral action in the exact quantum-mechanical FFCF, with respect to the difference between the forward and backward paths.[88] This leads to a classical-like expression for the FFCF, where the classical variables are replaced by certain Wigner transforms of the corresponding quantum-mechanical operators. We have also introduced a local harmonic approximation (LHA) in order to evaluate these Wigner transforms in many-body anharmonic systems.[83] In the remainder of this paper, we will refer to the method that results from the combination of the LSC and LHA approximations as LHA-LSC.

In previous work, we have demonstrated the accuracy of the LHA-LSC method on several nontrivial benchmark problems.[83] The feasibility of applying the method to molecular liquids was also demonstrated via applications to neat liquid oxygen, neat liquid nitrogen, and liquid oxygen/argon mixtures.[83−85] In all of these cases, we found the LHA-LSC-based predictions to be

* Corresponding author. E-mail: eitan@umich.edu.

10.1021/jp063907d CCC: $33.50
Published on Web 11/16/2006

in good agreement with the experimental results. This represented a dramatic improvement in comparison to the classical predictions, which are smaller than the experimental results by many orders of magnitude.

In a more recent paper, we reported the first application of the LHA-LSC method for calculating VER rates in a polyatomic system. The latter corresponded to a rigid, symmetrical, and linear triatomic molecule (A-B-A) in a monatomic liquid.[86] In this case, VER from the first excited state of the asymmetric stretch can occur either directly to the ground state or indirectly via intramolecular vibrational relaxation (IVR) to the first excited state of the symmetric stretch. The results reported in ref 86 gave rise to the following observations: (1) Generally speaking, VER rates predicted by the LSC method were faster than the classical ones. (2) The quantum enhancement of intermolecular VER was significantly stronger than that of IVR. (3) In cases where the A and B atoms were similar in mass, we found that while the classical VER rate in argon was faster than that in neon, at the same thermodynamic point in terms of reduced LJ units, the opposite trend was observed in the case of the LSC-based VER rates.

At the same time, *IVR was observed to be the preferred VER pathway of the excited asymmetric stretch, regardless of which method was used to calculate the rates (LHA-LSC or fully classical)*. The question addressed in the present paper is whether there could be cases where the preferred VER pathway predicted via the LHA-LSC method is different from that predicted by the classical treatment? To this end, we calculated the rates of the above-mentioned two different VER pathways in cases involving terminal *A* atoms that are increasingly more massive than the central B atom. This was motivated by the fact that the gap between the asymmetric stretch frequency and the IVR frequency becomes smaller with the increasing mass of the terminal A atom. Thus, the fact that the quantum rate enhancement of intermolecular VER is larger than that of IVR may makes it possible for the former to become the dominant VER pathway.

The remainder of this paper is organized as follows. The model Hamiltonian, general VER theory, and LHA-LSC method are outlined in Section II. The simulation parameters and techniques are outlined in Section III. The simulation results are reported and discussed in Section IV. We conclude in Section V.

II. Theory

In this section, we restrict ourselves to a brief outline of the model and VER theory (a more detailed discussion of these issues is available in ref 86). We consider a *rigid*, linear, and symmetric triatomic molecule A-B-A with the following vibrational Hamiltonian:

$$H_s = \frac{p_s^2}{2} + \frac{p_{as}^2}{2} + \frac{1}{2}\omega_s^2 q_s^2 + \frac{1}{2}\omega_{as}^2 q_{as}^2 \tag{1}$$

Here, (q_s,p_s) and (q_{as},p_{as}) are the *symmetric* stretch and *asymmetric* stretch mass-weighted normal-mode coordinates and momenta, respectively. ω_s and ω_{as} are the corresponding frequencies, explicitly given by

$$\omega_s = \sqrt{\kappa/m_A}, \quad \omega_{as} = \sqrt{\kappa M/m_A m_B} \tag{2}$$

where, κ is the A−B bond spring constant and $M = 2m_A + m_B$ is the molecular mass. It should be noted that

$$\frac{\omega_{as}}{\omega_s} = \sqrt{\frac{M}{m_B}} = \sqrt{1 + 2\frac{m_A}{m_B}} \tag{3}$$

such that $\omega_{as} > \omega_s$. The vibrational energy levels are given by

$$E_{n_s,n_{as}} = n_s\hbar\omega_s + n_{as}\hbar\omega_{as} \tag{4}$$

with n_s, $n_{as} = 0,1,2,...$ and such that $H_s|n_s, n_{as}\rangle = E_{n_s,n_{as}}|n_s, n_{as}\rangle$.

The solvent is assumed to be monatomic. The solvent−solvent interactions and the interactions between the solvent atoms and the three sites of the triatomic solute are described in terms of pair potentials. In actual simulations, we have assumed that all of these pair potentials are of the Lennard-Jones (LJ) type. The overall solute + solvent Hamiltonian is assumed to be given in the following form:

$$H = H_s + H_b + \mathbf{F}\cdot\mathbf{q} + \mathbf{q}^T\cdot\mathbf{G}\cdot\mathbf{q} \tag{5}$$

Here, H_b is the Hamiltonian of the non-vibrational DOF, $\mathbf{q} = (q_s,q_{as})$, and $\mathbf{F}\cdot\mathbf{q} + \mathbf{q}^T\cdot\mathbf{G}\cdot\mathbf{q}$ is the coupling between the vibrational modes and non-vibrational DOF. It should be noted that the coupling includes terms up to second order in $\mathbf{q}$. Explicit expressions for the matrix elements of $\mathbf{F}$ and $\mathbf{G}$ can be found in ref 86.

Starting at the first excited-state of the *asymmetric* stretch, $|0,1\rangle$, VER can follow one of two pathways:

1. Direct VER to the $|0,0\rangle$ state with the rate constant

$$k_{as} = \frac{1}{2\hbar\omega_{as}}\int_{-\infty}^{\infty} dt e^{-i\omega_{as}t} C_{as}(t) \tag{6}$$

where

$$C_{as}(t) = Z_b^{-1} Tr\{e^{-\beta H_b} e^{iH_b t/\hbar}\delta F_{as} e^{-iH_b t/\hbar}\delta F_{as}\} \tag{7}$$

Here, $Z_b = Tr(e^{-\beta H_b})$ and $\delta F_{as} = F_{as} - Z_b^{-1}Tr(e^{-\beta H_b}F_{as})$.

2. IVR to the $|1,0\rangle$ state with the rate constant

$$k_{ivr} = \frac{1}{4\omega_{as}\omega_s}\int_{-\infty}^{\infty} dt e^{-i\omega_{ivr}t} C_{ivr}(t) \tag{8}$$

where $\omega_{ivr} = \omega_{as} - \omega_s$, and

$$C_{ivr}(t) = Z_b^{-1} Tr\{e^{-\beta H_b} e^{iH_b t/\hbar}\delta G_{s,as} e^{-iH_b t/\hbar}\delta G_{s,as}\} \tag{9}$$

This process is followed by direct VER from the $|1,0\rangle$ state to the $|0,0\rangle$ state with the rate constant

$$k_s = \frac{1}{2\hbar\omega_s}\int_{-\infty}^{\infty} dt e^{-i\omega_s t} C_s(t) \tag{10}$$

where

$$C_s(t) = Z_b^{-1} Tr\{e^{-\beta H_b} e^{iH_b t/\hbar}\delta F_s e^{-iH_b t/\hbar}\delta F_s\} \tag{11}$$

Finally, we list below the expressions used for calculating the correlation functions, $C_s(t)$, $C_{as}(t)$, and $C_{ivr}(t)$ within the

framework of the LHA-LSC method (a detailed derivation of these results was provided in ref 86):

$$C_{as}(t) \approx \int d\mathbf{Q_0} \frac{\langle \mathbf{Q_0}|e^{-\beta H_b}|\mathbf{Q_0}\rangle}{Z_b} \int d\mathbf{P_{n,0}} \prod_{j=1}^{N} \left(\frac{1}{\alpha^{(j)}\pi\hbar^2}\right)^{1/2} \exp\left[-\frac{(P_{n,0}^{(j)})^2}{\hbar^2\alpha^{(j)}}\right] [\delta F_{as}(\mathbf{Q}_0) + D_{as}(\mathbf{Q}_0, \mathbf{P}_{n,0})]\delta F_{as}(\mathbf{Q}_t^{(Cl)}) \quad (12)$$

$$C_{s}(t) \approx \int d\mathbf{Q_0} \frac{\langle \mathbf{Q_0}|e^{-\beta H_b}|\mathbf{Q_0}\rangle}{Z_b} \int d\mathbf{P_{n,0}} \prod_{j=1}^{N} \left(\frac{1}{\alpha^{(j)}\pi\hbar^2}\right)^{1/2} \exp\left[-\frac{(P_{n,0}^{(j)})^2}{\hbar^2\alpha^{(j)}}\right] [\delta F_{s}(\mathbf{Q}_0) + D_{s}(\mathbf{Q}_0, \mathbf{P}_{n,0})]\, \delta F_{s}(\mathbf{Q}_t^{(Cl)}, \mathbf{P}_t^{(Cl)}) \quad (13)$$

$$C_{ivr}(t) \approx \int d\mathbf{Q_0} \frac{\langle \mathbf{Q_0}|e^{-\beta H_b}|\mathbf{Q_0}\rangle}{Z_b} \int d\mathbf{P_{n,0}} \prod_{j=1}^{N} \left(\frac{1}{\alpha^{(j)}\pi\hbar^2}\right)^{1/2} \exp\left[-\frac{(P_{n,0}^{(j)})^2}{\hbar^2\alpha^{(j)}}\right] [\delta G_{s,as}(\mathbf{Q}_0) + D_{s,as}(\mathbf{Q}_0, \mathbf{P}_{n,0})]\delta G_{s,as}(\mathbf{Q}_t^{(Cl)}) \quad (14)$$

Here, $\{P_n^{(k)}\}$ are mass-weighted normal-mode momenta, as obtained from the expansion of H_b to second order around $\mathbf{Q_0}$ (the LHA), and $\alpha^{(j)} = \Omega^{(j)}\coth[\beta\hbar\Omega^{(j)}/2]/\hbar$, where $\{(\Omega^{(k)})^2\}$ are the eigenvalues of the corresponding Hessian matrix. ($\mathbf{Q}_t^{(Cl)}$, $\mathbf{P}_t^{(Cl)}$) correspond to the classically propagated coordinates and momenta of the non-vibrational DOF, with the initial conditions ($\mathbf{Q_0}$, $\mathbf{P_0}$). The terms $D_{as}(\mathbf{Q_0}, \mathbf{P_{n,0}})$, $D_s(\mathbf{Q_0}, \mathbf{P_{n,0}})$, and $D_{s,as}(\mathbf{Q_0}, \mathbf{P_{n,0}})$ represent quantum nonlocality and vanish at the classical limit (explicit expressions for these terms can be found in ref 84). Another quantum-mechanical effect is introduced by the fact that the initial sampling of the positions and momenta is nonclassical. More specifically, the initial sampling of the positions is based on the exact quantum-mechanical position probability density, $\langle \mathbf{Q_0}|e^{-\beta H_b}|\mathbf{Q_0}\rangle/Z_b$, whereas the initial sampling of the momenta is based on the nonclassical probability density $\prod_{j=1}^{N}(1/(\alpha^{(j)}\pi\hbar^2))^{1/2}\exp[-((P_{n,0}^{(j)})^2)/(\hbar^2\alpha^{(j)})]$.

III. Model Parameters and Simulation Techniques

Classical and LHA-LSC-based calculations of k_s, k_{as}, and k_{ivr} were performed for three different solute molecules. The central B atom was assumed to have the mass of carbon, whereas the terminal A atoms were assumed to have the masses of oxygen, sulfur, or selenium. We will refer to these different triatomic solutes as CO_2, CS_2, and CSe_2 throughout the remainder of this paper. However, it should be emphasized that we do not expect our model to provide a realistic description of VER in the corresponding real molecules. The solvent is assumed to be monatomic and corresponds to either liquid argon or liquid neon at the same thermodynamic point in terms of reduced LJ units ($T^* = k_BT/\epsilon = 0.8$ and $\rho^* = \rho\sigma^3 = 0.85$, where T and ρ are the actual temperature and density and ϵ and σ are the usual LJ parameters). The model and simulation parameters are given in Table 1. The vibrational energy level diagrams for CO_2, CS_2, and CSe_2 are also drawn to scale in Figure 1, where it can be seen that ω_{as} *decreases* with increasing mass of the terminal atoms. It should be noted that the results for CO_2 in liquid argon and in liquid neon have already been reported in ref 86 and are only reproduced here for the sake of completeness.

TABLE 1: Model and Simulation Parameters[a]

model	CO_2/Ar	CO_2/Ne	CS_2/Ar	CS_2/Ne	CSe_2/Ar	CSe_2/Ne
r_e (Å)	1.16	1.16	1.56	1.56	1.71	1.71
m_A (amu)	16.0	16.0	32.0	32.0	79.0	79.0
m_B (amu)	12.0	12.0	12.0	12.0	12.0	12.0
$\omega_{as}/2\pi c$ (cm^{-1})	2400	2400	1686	1686	1326	1326
$\omega_s/2\pi c$ (cm^{-1})	1253	1253	670	670	352	352
$\omega_{ivr}/2\pi c$ (cm^{-1})	1147	1147	1016	1016	974	974
ϵ_s/k_B (K)	117.7	47.0	117.7	47.0	117.7	47.0
σ_s (Å)	3.504	2.72	3.504	2.72	3.504	2.72
ϵ_A/k_B (K)	85.1	53.8	146.8	92.7	146.8	92.7
σ_A (Å)	3.23	2.84	3.512	3.12	3.552	3.16
ϵ_B/k_B (K)	77.6	49.1	77.6	49.1	77.6	49.1
σ_B (Å)	3.43	3.04	3.43	3.04	3.43	3.04
T (K)	94.16	37.6	94.16	37.6	94.16	37.6
ρ (nm^{-3})	19.76	42.24	19.76	42.24	19.76	42.24
time step (fs)	4.0	3.0	4.0	3.0	4.0	3.0

[a] All simulations were performed with one triatomic solute and 105 solvent atoms in the simulation box.

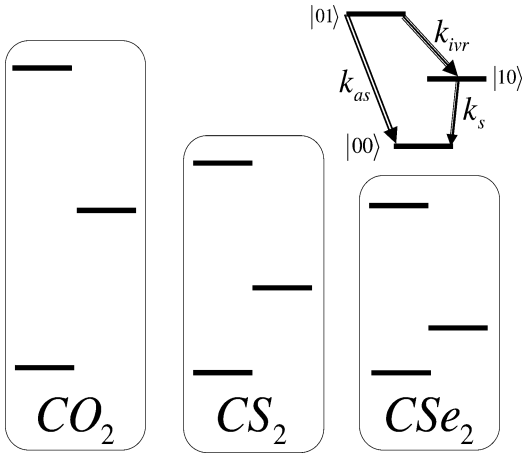

Figure 1. Vibrational energy level diagrams for CO_2, CS_2, and CSe_2 (drawn to scale). It should be noted that ω_{as} *decreases* as decreases with increasing mass of the terminal atoms. Also shown is a schematic view of the VER pathways considered in this paper.

The LJ parameters for the solvent−solute interaction were obtained via the Lorentz−Berthelot mixing rules, with $\sigma_C = 0.335$ nm, $\sigma_O = 0.295$ nm, $\sigma_S = 0.352$ nm, $\sigma_{Se} = 0.36$ nm, $\sigma_{Ar} = 0.3054$ nm, $\sigma_{Ne} = 0.272$ nm, $\epsilon_C/k_B = 51.12$ K, $\epsilon_O/k_B = 61.6$ K, $\epsilon_S/k_B = 183$ K, $\epsilon_{Se}/k_B = 183$ K, $\epsilon_{Ar}/k_B = 117.7$ K, and $\epsilon_{Ne}/k_B = 47$ K.[89,90] It should be noted that we have assumed that the Se−Se interaction strength is similar to the S−S interaction strength,[91] and that as a result $\epsilon_{Se} \approx \epsilon_S$. The values of the A−B bond length, r_e, and ω_{as} for CO_2 were adopted from ref 92, and the corresponding value of ω_s was calculated with the help of eq 3. The values of r_e and ω_s for CS_2 were adopted from ref 93 and the corresponding value of ω_{as} was calculated with the help of eq 3. The value of r_e for CSe_2 was adopted from ref 94, and the corresponding values of ω_s and ω_{as} were calculated from the value of $2\omega_s + \omega_{as} = 2031$ cm^{-1} (cf. ref 94) and eq 3. The above values of ω_s and ω_{as} were also found to be within ~100 cm^{-1} of these calculated for the isolated molecules via DFT.

The simulation procedures used are the same as these described in ref 86 for CO_2 in argon and neon. A cubical simulation cell with a single triatomic solute and 105 solvent atoms was used. For the classical simulations, the system was equilibrated via the velocity rescaling method and propagated in time via the velocity Verlet method.[89] Classical simulations on the CSe_2/Ne system were started by replacing the CO_2 molecule by CSe_2 in an equilibrium configuration of the CO_2/

TABLE 2: k_{as}, k_s, and k_{ivr} in the CO_2/Ar System, as Obtained via the LHA-LSC Method[a]

CO_2/Ar	k_{as}/s^{-1}	k_s/s^{-1}	k_{ivr}/s^{-1}
classical	$(6 \pm 1) \times 10^{-15}$	$(1.4 \pm 0.1) \times 10^{-1}$	$(1.17 \pm 0.04) \times 10^{-2}$
LHA-LSC	$(4 \pm 1) \times 10^{-7}$	$(1.1 \pm 0.1) \times 10^{3}$	$(6 \pm 1) \times 10^{-1}$
standard QCF	$(1.2 \pm 0.2) \times 10^{-14}$	$(2.8 \pm 0.2) \times 10^{-1}$	$(2.34 \pm 0.08) \times 10^{-2}$
harmonic QCF	$(2.2 \pm 0.4) \times 10^{-13}$	2.7 ± 0.2	0.203 ± 0.007
Schofield QCF	$(5.5 \pm 0.9) \times 10^{-7}$	$(2.0 \pm 0.1)10^{3}$	75 ± 3
MHS QCF	$(3.5 \pm 0.6) \times 10^{-10}$	73 ± 5	3.9 ± 0.1

[a] Also shown are the corresponding predictions obtained via fully classical simulations, and by using the following QCFs ($x = \beta\hbar\omega$):[87] (1) standard: $f_{st}(x) = 2/(1 + e^{-x})$; (2) harmonic: $f_h(x) = x/(1 - e^{-x})$; (3) Schofield: $f_{Sc} = e^{x/2}$; and (4) mixed harmonic/Schofield (MHS): $f_{MHS}(x) = \sqrt{xe^{x/2}/(1-e^{-x})}$.

TABLE 3: Same as Table 2, for the CO_2/Ne System

CO_2/Ne	k_{as}/s^{-1}	k_s/s^{-1}	k_{ivr}/s^{-1}
classical	$(2.4 \pm 0.8) \times 10^{-19}$	$(5 \pm 1) \times 10^{-4}$	$(9.9 \pm 0.8) \times 10^{-5}$
LHA-LSC	$(1.5 \pm 0.4) \times 10^{-4}$	$(1.0 \pm 0.2) \times 10^{4}$	2.6 ± 0.4
standard QCF	$(5 \pm 2) \times 10^{-19}$	$(1.0 \pm 0.2) \times 10^{-3}$	$(2.0 \pm 0.2) \times 10^{-4}$
harmonic QCF	$(2.2 \pm 0.3) \times 10^{-17}$	$(2.4 \pm 0.5) \times 10^{-2}$	$(4.3 \pm 0.8) \times 10^{-3}$
Schofield QCF	23 ± 8	$(1.3 \pm 0.3) \times 10^{7}$	$(3.4 \pm 0.3) \times 10^{5}$
MHS QCF	$(2.2 \pm 0.7) \times 10^{-8}$	$(6 \pm 1) \times 10^{2}$	38 ± 3

TABLE 4: Same as Table 2, for the CS_2/Ar System

CS_2/Ar	k_{as}/s^{-1}	k_s/s^{-1}	k_{ivr}/s^{-1}
classical	$(4.8 \pm 0.7) \times 10^{-12}$	$(2.26 \pm 0.09) \times 10^{3}$	$(8 \pm 2) \times 10^{-5}$
LHA-LSC	$(1.4 \pm 0.6) \times 10^{-5}$	$(2.3 \pm 0.3) \times 10^{5}$	$(8 \pm 3) \times 10^{-3}$
standard QCF	$(10 \pm 1) \times 10^{-12}$	$(4.5 \pm 0.2) \times 10^{3}$	$(1.6 \pm 0.4) \times 10^{-4}$
harmonic QCF	$(1.2 \pm 0.2) \times 10^{-10}$	$(2.31 \pm 0.9) \times 10^{4}$	$(1.2 \pm 0.3) \times 10^{-3}$
Schofield QCF	$(1.9 \pm 0.3) \times 10^{-6}$	$(3.8 \pm 0.1) \times 10^{5}$	$(1.9 \pm 5) \times 10^{-1}$
MHS QCF	$(1.5 \pm 0.2) \times 10^{-8}$	$(9.3 \pm 0.4) \times 10^{4}$	$(1.5 \pm 0.4) \times 10^{-2}$

Ne system. This was followed by equilibration over 15 ns. A similar procedure was used for the classical simulation of the CSe_2/Ar, CS_2/Ar and CS_2/Ne systems (except for the fact that equilibration of the latter two systems was started at an equilibrium configuration of CSe_2 in the corresponding solvent).

The equilibration period was followed by a calculation of the classical correlations functions $C_s(t)$, $C_{as}(t)$, and $C_{ivr}(t)$ by averaging over $(4 - 10) \times 10^3$ trajectories, each with 5000 time steps. Once the classical correlation functions were obtained, their FT was calculated via the FFT method. In the case of very high vibrational frequencies (>300 cm^{-1}) the FT is a very small number, and therefore very difficult to compute directly. Following the common practice, we instead extrapolated the exponential gap law, which was observed to emerge at low frequencies, to higher frequencies.[95,96] Assuming that this extrapolation is the major source of error, we evaluated the error bars reported for the VER rate constants based on the least-squares fit to the corresponding linear frequency dependence of the VER rate constant (on a semilog scale).

LHA-LSC-based calculations of k_s, k_{as}, and k_{ivr} start by sampling the initial positions of all the atoms in the simulation cell via a PIMD simulation, where 16 beads were assigned to each atom. The PIMD simulation was started with all 16 beads in the position of the corresponding atom in a classical equilibrium configuration (as obtained from the classical simulation described in the previous paragraphs). This was followed by an equilibration period of 2.7 ps (Ne) or 3.6 ps (Ar) at the desired temperatures, with the help of Nosé−Hoover chain thermostats of length four (one thermostat for each of the three Cartesian coordinates of each atom) and the velocity Verlet algorithm.[97] It should be noted that the initial configurations sampled satisfied the constraint imposed by the linearity of the triatomic molecule.[84] The sampling was performed by choosing random beads from snapshots of the isomorphic liquid of cyclic polymers at each time step. An overall number of about 3×10^5 initial configurations was used. For each of these, we calculated the normal-mode frequencies and transformation matrix via the Jacobi method,[98] and used them in order to sample the initial normal-mode momenta. Here too, we restrict ourselves to normal-mode displacements that satisfy the constraints imposed by the linearity of the triatomic molecule.[84] We then performed a classical MD simulation over 500 time steps for each of the initial configurations, and extracted the correlation functions $C_s(t)$, $C_{as}(t)$, and $C_{ivr}(t)$ from them. It should be noted that in calculating correlations functions via LHA-LSC, we can only correlate the relevant quantities at $t = 0$ and at a later time t. All of the results reported below were based on the cosine transform of the real part of the correlation functions.[85]

IV. Results and Discussion

The values of k_{as}, k_s, and k_{ivr}, as obtained via the classical and LHA-LSC-based treatments for all six combinations of the three solutes (CO_2, CS_2 and CSe_2) and two solvents (argon and neon), are given in Tables 2−7. The VER rate constants k_{as}, k_s, and k_{ivr} for the CS_2/Ar, CS_2/Ne, CSe_2/Ar and CSe_2/Ne systems are also shown in Figures 2−5, as a function of frequency and on a semilog plot (the corresponding figures for the CO_2/Ar and CO_2/Ne systems can be found in ref 86).

The following observations can be made based on the results presented in Tables 2−7:

- Generally speaking, the VER rate constants predicted by the LHA-LSC method are faster than those predicted by the classical treatment. A similar quantum enhancement of VER rates has been observed in other nonpolar liquid solutions and is attributed to the ability to penetrate classically forbidden areas on the repulsive region of the interaction potential.[83−85]

- The quantum enhancement factor in liquid neon is larger than that in liquid argon. This leads to an interesting trend reversal in the solvent dependence of VER rates between the classical and LHA-LSC-based treatments. More specifically, although the classical VER rates in liquid argon are faster than

TABLE 5: Same as Table 2, for the CS_2/Ne System

CS_2/Ne	k_{as}/s^{-1}	k_s/s^{-1}	k_{ivr}/s^{-1}
classical	$(2.0 \pm 0.3) \times 10^{-14}$	86 ± 6	$(2.3 \pm 0.3) \times 10^{-7}$
LHA-LSC	$(4 \pm 2) \times 10^{-3}$	$(18 \pm 3) \times 10^{5}$	$(1.2 \pm 0.1) \times 10^{-1}$
standard QCF	$(4.0 \pm 0.6) \times 10^{-14}$	$(1.7 \pm 0.1) \times 10^{2}$	$(4.6 \pm 0.6) \times 10^{-7}$
harmonic QCF	$(1.3 \pm 0.2) \times 10^{-12}$	$(2.2 \pm 0.2) \times 10^{3}$	$(9 \pm 1) \times 10^{-6}$
Schofield QCF	2.1 ± 0.3	$(3.3 \pm 0.2) \times 10^{7}$	64 ± 8
MHS QCF	$(1.7 \pm 0.3) \times 10^{-6}$	$(2.7 \pm 0.2) \times 10^{5}$	$(2.4 \pm 0.3) \times 10^{-2}$

TABLE 6: Same as Table 2, for the CSe_2/Ar System

CSe_2/Ar	k_{as}/s^{-1}	k_s/s^{-1}	k_{ivr}/s^{-1}
classical	$(3.1 \pm 0.6) \times 10^{-9}$	$(3.2 \pm 0.1) \times 10^{6}$	$(4.7 \pm 0.6) \times 10^{-7}$
LHA-LSC	$(2.5 \pm 0.8) \times 10^{-4}$	$(4.9 \pm 0.7) \times 10^{7}$	$(3 \pm 1) \times 10^{-6}$
standard QCF	$(6 \pm 1) \times 10^{-9}$	$(6.4 \pm 0.2) \times 10^{6}$	$(9 \pm 1) \times 10^{-7}$
harmonic QCF	$(6 \pm 1) \times 10^{-8}$	$(1.7 \pm 0.1) \times 10^{7}$	$(7 \pm 1) \times 10^{-6}$
Schofield QCF	$(8 \pm 2) \times 10^{-5}$	$(4.7 \pm 0.1) \times 10^{7}$	$(8 \pm 1) \times 10^{-4}$
MHS QCF	$(2.2 \pm 0.4) \times 10^{-6}$	$(2.8 \pm 0.1) \times 10^{7}$	$(8 \pm 1) \times 10^{-5}$

TABLE 7: Same as Table 2, for the CSe_2/Ne System

CSe_2/Ne	k_{as}/s^{-1}	k_s/s^{-1}	k_{ivr}/s^{-1}
classical	$(5 \pm 1) \times 10^{-10}$	$(9.9 \pm 0.3) \times 10^{5}$	$(2.0 \pm 0.8) \times 10^{-8}$
LHA-LSC	$(2.7 \pm 0.5) \times 10^{-1}$	$(1.4 \pm 0.1) \times 10^{8}$	$(9 \pm 4) \times 10^{-5}$
standard QCF	$(10 \pm 2) \times 10^{-10}$	$(19.8 \pm 0.6) \times 10^{5}$	$(4.0 \pm 2) \times 10^{-8}$
harmonic QCF	$(2.5 \pm 0.5) \times 10^{-8}$	$(1.34 \pm 0.04) \times 10^{7}$	$(7 \pm 3) \times 10^{-7}$
Schofield QCF	50 ± 10	$(8.5 \pm 0.3) \times 10^{8}$	3 ± 1
MHS QCF	$(1.2 \pm 0.3) \times 10^{-3}$	$(1.06 \pm 0.03) \times 10^{8}$	$(1.4 \pm 0.4) \times 10^{-3}$

these in liquid neon, the opposite is true for the LHA-LSC-based VER rates. This implies that the reduction of the VER rates due to the lower temperature of liquid neon is more than compensated for by a considerably larger quantum enhancement. This may be explained by the fact that neon has a smaller mass than argon and that the solute−solvent interaction potentials in the repulsive region are somewhat softer in the case of neon than in the case of argon. This better ability to penetrate classically forbidden areas on the repulsive region of the interaction potential in the neon solvent gives rise to a larger quantum enhancement. The fact that the trend reversal becomes less pronounced with increasing mass of the terminal A atom is also consistent with this interpretation.

- The quantum enhancement of the VER rates is clearly pathway-dependent. The largest quantum enhancement is observed in the case of k_{as}, followed by a significantly smaller quantum enhancement of k_s, and yet a smaller quantum

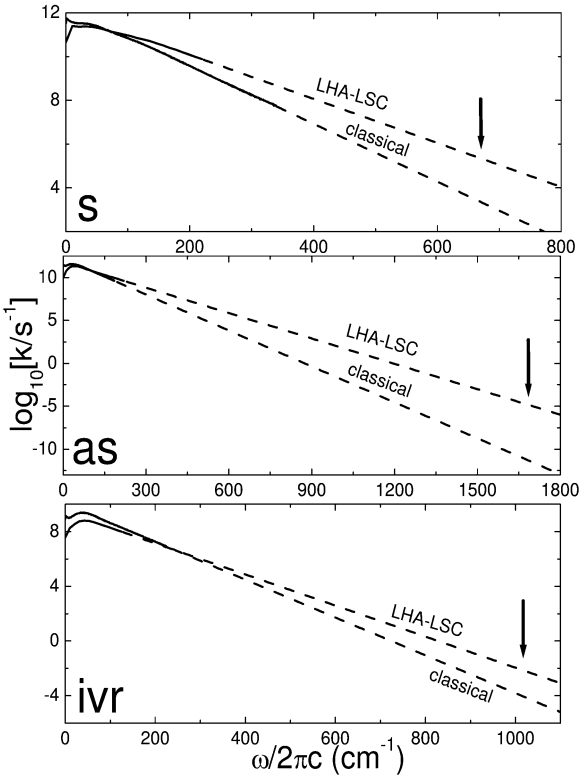

Figure 2. Classical and LHA-LSC frequency-dependent rate constants for the symmetric stretch, asymmetric stretch, and IVR for CS_2 in argon. Calculated data are shown as solid lines. The dashed lines represent extrapolations to the corresponding frequencies of the symmetric and asymmetric stretches. The relevant frequencies are indicated by arrows.

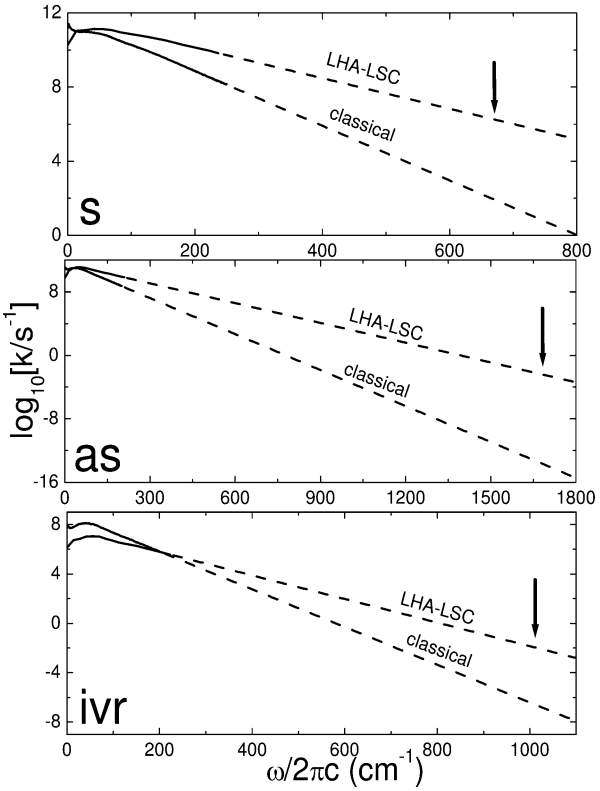

Figure 3. Same as Figure 2, for CS_2 in neon.

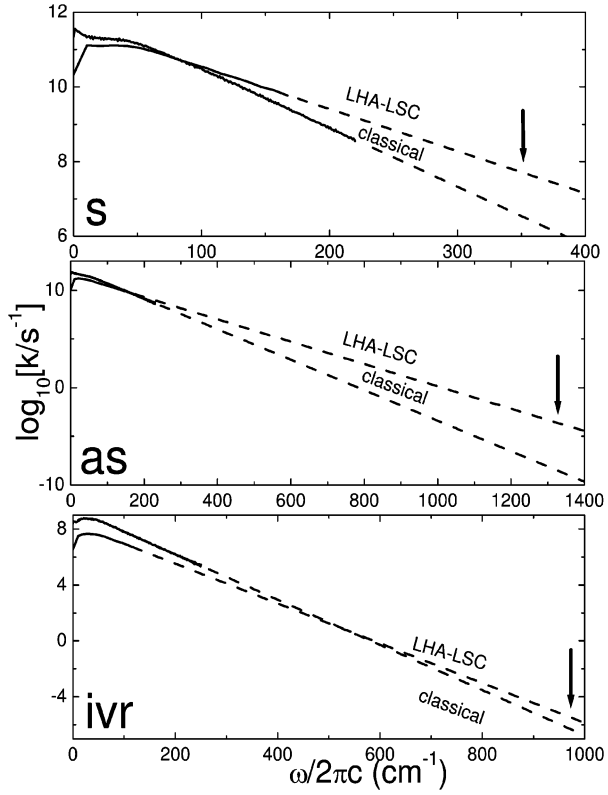

Figure 4. Same as Figure 2, for CSe_2 in argon.

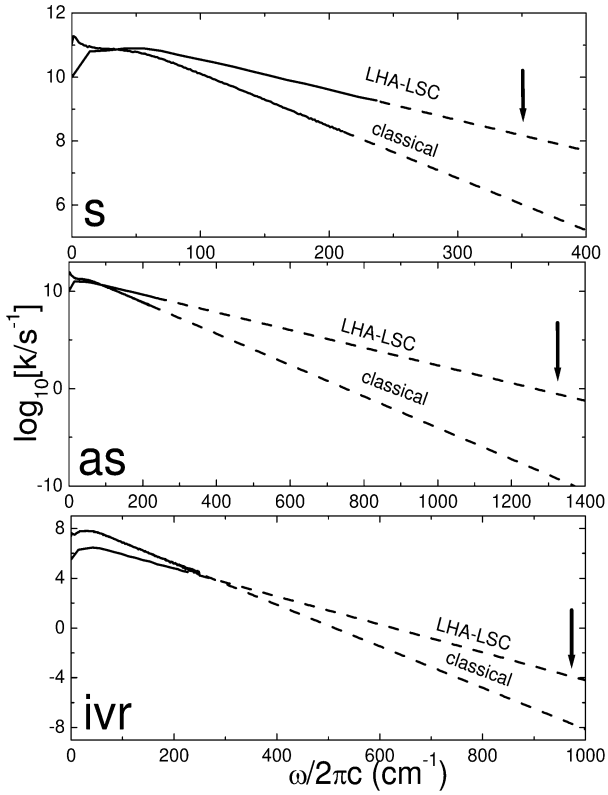

Figure 5. Same as Figure 2, for CSe_2 in neon.

enhancement of k_{ivr}. These differences may be attributed to the fact that the solvent is more effective at assisting VER of the asymmetric stretch than it is in assisting VER of the symmetric stretch, and even less so when it comes to assisting IVR.[74]

• Although IVR is the preferred *classical* pathway in all of the cases considered here, this is not the case when LHA-LSC is used for calculating the VER rates. This is because the larger quantum enhancement of k_{as} in comparison to k_{ivr} decreases the gap between these two rate constants. In fact, the semiclassical k_{as} may even become faster than k_{ivr}, such that intermolecular VER will become the preferred VER pathway, as is indeed observed in the case of CSe_2.

The first three observations reinforce similar observations from our previous study.[86] However, to the best of our knowledge, the fourth observation represents the first reported example of a situation where the quantum VER pathway differs from the classical one. It is important to note that this trend reversal relies on the third observation, according to which the quantum enhancement of solvent-assisted IVR is orders of magnitude weaker than that of intermolecular VER.

It is also interesting to compare the results obtained using the LHA-LSC method to those obtained by using QCFs. In this case, one "corrects" the classical VER rate constant by multiplying it by a frequency-dependent QCF, that is, $k_j \approx f(\beta\hbar\omega)k_j^{(Cl)}$, where j = s,as,ivr.[87] The VER rate constants obtained by using different QCFs are reported in Tables 2−7. The following observations can be made based on these results:

• From the four QCFs considered, the Schofield and Mixed Harmonic-Schofield (MHS) QCFs lead to VER rate constants that are the closest to those obtained via the LHA-LSC method. It should be noted that the quantum enhancement of the VER rate predicted by the Schofield and MHS QCFs is significantly larger than that predicted by the Standard and Harmonic QCFs.

• In the case of liquid argon solutions, the values of k_{as} and k_s obtained by using the LHA-LSC method are closest to these obtained by using the Schofield QCF, whereas the values of k_{ivr} obtained by using the LHA-LSC method are closest to these obtained by using the MHS QCF. It should be noted that the Schofield QCF is generally larger than the MHS QCF. This observation is therefore consistent with the fact that LHA-LSC predicts a stronger quantum enhancement of intermolecular VER.

• A similar trend is seen in the case of liquid neon solutions, where LHA-LSC predicts a weaker quantum enhancement of IVR in comparison to intermolecular VER.

• All of the QCFs point to IVR as the preferred VER pathway in the case of CSe_2/Ar, which should be contrasted with the prediction of LHA-LSC that intermolecular VER is the preferred pathway in this case.

• The different QCFs predict different preferred VER pathways in the case of CSe_2/Ne. More specifically, the Schofield QCF points to intermolecular VER as the preferred pathway (similar to the LHA-LSC method), the MHS QCF predicts similar rates for IVR and intermolecular VER, and the other QCFs predict that IVR is the preferred pathway.

V. Concluding Remarks

In this paper, we have shown that the preferred VER pathway predicted via the LHA-LSC method can be different from that predicted by the classical treatment. The example of CSe_2 in liquid argon or neon, where IVR is the preferred *classical* pathway and direct intermolecular VER to the ground state is the preferred pathway within the framework of the LHA-LSC method, demonstrates this point. This trend reversal originates from the weaker quantum enhancement of solvent-assisted IVR in comparison to intermolecular VER. It should be noted that a similar trend is predicted by the Schofield QCF in the case of CSe_2 in liquid neon.

One may obviously question the accuracy of the LHA-LSC method for the system considered here and its ability to capture all relevant quantum effects. Unfortunately, addressing this

question systematically would require a comparison to the exact quantum-mechanical VER rate constants, which cannot be computed for the type of system considered here. A less systematic, yet presumably more feasible, alternative approach could be based on comparison to experiment. However, a truly realistic model for VER in CO_2, CS_2, and CSe_2 will require more accurate force fields and would have to include stretch-to-bend VER pathways, intramolecular anharmonic coupling terms, and higher order IVR processes. At the same time, it is also important to note that the accuracy of the LHA-LSC method has been demonstrated on several nontrivial benchmark problems for which the exact quantum-mechanical FFCF can be computed, and that its predictions compared well with experimental VER rates measured in other nonpolar liquid solutions.[83−85] It should also be noted that the LHA-LSC method *predicts* the variations in quantum rate enhancement between different VER pathways. This should be contrasted with the QCF approach, where observing the same effect would require *assigning* different QCFs to different VER pathways. Finally, it should be noted that although the model Hamiltonian is probably too oversimplified for describing VER in the real CO_2, CS_2, and CSe_2 molecules, it is nevertheless self-consistent and therefore sufficient for a proof-of-principle demonstration that the quantum and classical VER pathways can differ.

The next step is clearly to extend the analysis to more realistic models, so as to make it possible to perform direct comparison to experimental data. To this end, it would be important to also account for stretch-to-bend VER pathways, higher order IVR processes, and polar solute−solvent interactions. The investigation of these issues is currently underway in our group and will be reported in future publications.

Acknowledgment. We are grateful for financial support from the National Science Foundation through grant no. CHE-0306695. We also thank Mr. Nick Preketes for DFT calculations of the frequencies of the symmetric and asymmetric stretches in CO_2, CS_2, and CSe_2.

References and Notes

(1) Calaway, W. F.; Ewing, G. E. *J. Chem. Phys.* **1975**, *63*, 2842.
(2) Brueck, S. R. J.; Osgood, R. M. *Chem. Phys. Lett.* **1976**, *39*, 568.
(3) Chateau, M.; et al. *J. Chem. Phys.* **1979**, *71*, 4799.
(4) Delalande, C.; Gale, G. M. *J. Chem. Phys.* **1979**, *71*, 4804.
(5) Delalande, C.; Gale, G. M. *J. Chem. Phys.* **1980**, *73*, 1918.
(6) Faltermeier, B.; Protz, R.; Maier, M.; Werner, E. *Chem. Phys. Lett.* **1980**, *74*, 425.
(7) Faltermeier, B.; Protz, R.; Maier, M. *Chem. Phys.* **1981**, *62*, 377.
(8) Oxtoby, D. W. *Adv. Chem. Phys.* **1981**, *47* (Part 2), 487.
(9) Roussignol, P.; Delalande, C.; Gale, G. M. *Chem. Phys.* **1982**, *70*, 319.
(10) Heilweil, E. J.; Doany, F. E.; Moore, R.; Hochstrasser, R. M. *J. Chem. Phys.* **1982**, *76*, 5632.
(11) Oxtoby, D. W. *Annu. Rev. Phys. Chem.* **1981**, *32*, 77.
(12) Oxtoby, D. W. *J. Phys. Chem.* **1983**, *87*, 3028.
(13) Chesnoy, J.; Gale, G. M. *Ann. Phys. Fr.* **1984**, *9*, 893.
(14) Heilweil, E. J.; Casassa, M. P.; Cavanagh, R. R.; Stephenson, J. C. *Chem. Phys. Lett.* **1985**, *117*, 185.
(15) Heilweil, E. J.; Casassa, M. P.; Cavanagh, R. R.; Stephenson, J. C. *J. Chem. Phys.* **1986**, *85*, 5004.
(16) Paige, M. E.; Russell, D. J.; Harris, C. B. *J. Chem. Phys.* **1986**, *85*, 3699.
(17) Harris, A. L.; Brown, J. K.; Harris, C. B. *Annu. Rev. Phys. Chem* **1988**, *39*, 341.
(18) Chesnoy, J.; Gale, G. M. *Adv. Chem. Phys.* **1988**, *70* (part 2), 297.
(19) Harris, C. B.; Smith, D. E.; Russell, D. J. *Chem. Rev.* **1990**, *90*, 481.
(20) Paige, M. E.; Harris, C. B. *Chem. Phys.* **1990**, *149*, 37.
(21) Owrutsky, J. C.; et al. *Chem. Phys. Lett.* **1991**, *184*, 368.
(22) Elsaesser, T.; Kaiser, W. *Annu. Rev. Phys. Chem.* **1991**, *42*, 83.
(23) Moustakas, A.; Weitz, E. *J. Chem. Phys.* **1993**, *98*, 6947.
(24) Kliner, D. A. V.; Alfano, J. C.; Barbara, P. F. *J. Chem. Phys.* **1993**, *98*, 5375.
(25) Zimdars, D.; et al. *Phys. Rev. Lett.* **1993**, *70*, 2718.
(26) Miller, D. W.; Adelman, S. A. *Int. Rev. Phys. Chem.* **1994**, *13*, 359.
(27) Owrutsky, J. C.; Raftery, D.; Hochstrasser, R. M. *Annu. Rev. Phys. Chem.* **1994**, *45*, 519.
(28) Salloum, A.; Dubost, H. *Chem. Phys.* **1994**, *189*, 179.
(29) Tokmakoff, A.; Sauter, B.; Fayer, M. D. *J. Chem. Phys.* **1994**, *100*, 9035.
(30) Tokmakoff, A.; Fayer, M. D. *J. Chem. Phys.* **1995**, *103*, 2810.
(31) Pugliano, N.; Szarka, A. Z.; Gnanakaran, S.; Hochstrasser, R. M. *J. Chem. Phys.* **1995**, *103*, 6498.
(32) Owrutsky, J. C.; Li, M.; Locke, B.; Hochstrasser, R. M. *J. Phys. Chem.* **1995**, *99*, 4842.
(33) Stratt, R. M.; Maroncelli, M. *J. Phys. Chem.* **1996**, *100*, 12981.
(34) Urdahl, R. S.; et al. *J. Chem. Phys.* **1997**, *107*, 3747.
(35) Myers, D. J.; Urdahl, R. S.; Cherayil, B. J.; Fayer, M. D. *J. Chem. Phys.* **1997**, *107*, 9741.
(36) Hamm, P.; Lim, M.; Hochstrasser, R. M. *J. Chem. Phys.* **1997**, *107*, 1523.
(37) Laenen, R.; Rauscher, C.; Laubereau, A. *Phys. Rev. Lett.* **1998**, *80*, 2622.
(38) Myers, D. J.; et al. *J. Chem. Phys.* **1998**, *109*, 5971.
(39) Sagnella, D. E.; et al. *Proc. Natl. Acad. Sci. U.S.A.* **1999**, *96*, 14324.
(40) Deng, Y.; Stratt, R. M. *J. Chem. Phys.* **2002**, *117*, 10752.
(41) Li, S.; Thompson, W. H. *J. Chem. Phys.* **2003**, *107*, 8696.
(42) Bakker, H. J. *J. Chem. Phys.* **2004**, *121*, 10088.
(43) Laubereau, A.; Kaiser, W. *Rev. Mod. Phys.* **1978**, *50*, 607.
(44) Graener, H.; Seifert, G.; Laubereau, A. *Phys. Rev. Lett.* **1991**, *66*, 2092.
(45) Vodopyanov, K. L. *J. Chem. Phys.* **1991**, *94*, 5389.
(46) Bakker, H. J. *J. Chem. Phys.* **1993**, *98*, 8496.
(47) Hofmann, M.; Graener, H. *Chem. Phys.* **1996**, *206*, 129.
(48) Graener, H.; R. Zürl, Hofmann, M. *J. Phys. Chem. B* **1997**, *101*, 1745.
(49) Hayes, S. C.; Philpott, M. J.; Reid, P. J. *J. Chem. Phys.* **1998**, *109*, 2596.
(50) Woutersen, S.; Emmerichs, U.; Nienhuys, H.; Bakker, H. J. *Phys. Rev. Lett.* **1998**, *81*, 1106.
(51) Deak, J. C.; Iwaki, L. K.; Dlott, D. D. *Chem. Phys. Lett.* **1998**, *293*, 405.
(52) Deak, J. C.; Iwaki, L. K.; Dlott, D. D. *J. Phys. Chem. A* **1998**, *102*, 8193.
(53) Iwaki, L. K.; Deak, J. D.; Rhea, S. T.; Dlott, D. D. *Chem. Phys. Lett.* **1999**, *303*, 176.
(54) Deak, J. C.; Iwaki, L. K.; Dlott, D. D. *J. Phys. Chem. A* **1999**, *103*, 971.
(55) Nienhuys, H.; Woutersen, S.; R. A. van Santen, Bakker, H. J. *J. Chem. Phys.* **1900**, *111*, 1494.
(56) Seifert, G.; R. Zürl, Graener, H. *J. Phys. Chem. A* **1999**, *103*, 10749.
(57) Seifert, G.; R. Zürl, Patzlaff, T.; Graener, H. *J. Chem. Phys.* **2000**, *112*, 6349.
(58) Deak, J. C.; Iwaki, L. K.; Rhea, S. T.; Dlott, D. D. *J. Raman Spectrosc.* **2000**, *31*, 263.
(59) Deak, J. C.; Rhea, S. T.; Iwaki, L. K.; Dlott, D. D. *J. Phys. Chem. A* **2000**, *104*, 4866.
(60) Iwaki, L. K.; Dlott, D. D. *Chem. Phys. Lett.* **2000**, *321*, 419.
(61) Iwaki, L. K.; Dlott, D. D. *J. Phys. Chem. A* **2000**, *104*, 9101.
(62) Dlott, D. D. *Chem. Phys.* **2001**, *266*, 149.
(63) Wang, Z.; Pakoulev, A.; Dlott, D. D. *Science* **2002**, *296*, 2201.
(64) Wang, Z.; Pakoulev, A.; Pang, Y.; Dlott, D. D. *Chem. Phys. Lett.* **2003**, *378*, 281.
(65) Pakoulev, A.; Wang, Z.; Dlott, D. D. *Chem. Phys. Lett.* **2003**, *371*, 2203.
(66) Pakoulev, A.; Wang, Z.; Pang, Y.; Dlott, D. D. *Chem. Phys. Lett.* **2003**, *380*, 404.
(67) Wang, Z.; Pakoulev, A.; Pang, Y.; Dlott, D. D. *J. Phys. Chem. A* **2004**, *108*, 9054.
(68) Wang, Z.; Pang, Y.; Dlott, D. D. *Chem. Phys. Lett.* **2004**, *397*, 40.
(69) Rey, R.; Hynes, J. T. *Chem. Rev.* **2004**, *104*, 1915.
(70) Lawrence, C. P.; Skinner, J. L. *J. Chem. Phys.* **2002**, *117*, 5827.
(71) Sibert, E. L., III; Rey, R. *J. Chem. Phys.* **2002**, *116*, 237.
(72) Gulmen, T. S.; Sibert, E. L., III *J. Phys. Chem. A* **2004**, *108*, 2389.
(73) Gulmen, T. S.; Sibert, E. L., III *J. Phys. Chem. A* **2005**, *109*, 5777.
(74) Deng, Y.; Stratt, R. M. *J. Chem. Phys.* **2002**, *117*, 1735.
(75) Chorny, I.; Vieceli, J.; Benjamin, I. *J. Chem. Phys.* **2002**, *116*, 8904.
(76) Rey, R.; Hynes, J. T. *J. Chem. Phys.* **1996**, *104*, 2356.
(77) Lawrence, C. P.; Skinner, J. L. *J. Chem. Phys.* **2003**, *119*, 1623.
(78) Ferrario, M.; Klein, M. L.; McDonald, I. R. *Chem. Phys. Lett.* **1993**, *213*, 537.
(79) Morita, A.; Kato, S. *J. Chem. Phys.* **1998**, *109*, 5511.

(80) Zwanzig, R. *J. Chem. Phys.* **1961**, *34*, 1931.
(81) Everitt, K. F.; Egorov, S. A.; Skinner, J. L. *Chem. Phys.* **1998**, *235*, 115.
(82) Everitt, K. F.; Skinner, J. L. *J. Chem. Phys.* **1999**, *110*, 4467.
(83) Shi, Q.; Geva, E. *J. Phys. Chem. A* **2003**, *107*, 9059.
(84) Shi, Q.; Geva, E. *J. Phys. Chem. A* **2003**, *107*, 9070.
(85) Ka, B. J.; Shi, Q.; Geva, E. *J. Phys. Chem. A* **2005**, *109*, 5527.
(86) Ka, B. J.; Geva, E. *J. Phys. Chem. A* **2006**, *110*, 9555.
(87) Skinner, J. L.; Park, K. *J. Phys. Chem. B* **2001**, *105*, 6716.
(88) Shi, Q.; Geva, E. *J. Chem. Phys.* **2003**, *118*, 8173.
(89) Allen, M. P.; Tildesley, D. J. *Computer Simulation of Liquids*; Clarendon: Oxford, 1987.
(90) Lowden, L. J.; Chandler, D. *J. Chem. Phys.* **5228**, *61*, 46.
(91) Jovari, P. *Mol. Phys.* **1999**, *97*, 1149.
(92) Velsko, S.; Oxtoby, D. W. *Chem. Phys. Lett.* **1980**, *69*, 462.
(93) Martin, J. M. L.; Francois, J.; Gijbels, R. *J. Mol. Spectrosc.* **1995**, *169*, 445.
(94) Maki, A. G.; Sams, R. L. *J. Mol. Spectrosc.* **1981**, *90*, 215.
(95) Nitzan, A.; Mukamel, S.; Jortner, J. *J. Chem. Phys.* **1974**, *60*, 3929.
(96) Nitzan, A.; Mukamel, S.; Jortner, J. *J. Chem. Phys.* **1975**, *63*, 200.
(97) Jang, S.; Voth, G. A. *J. Chem. Phys.* **1997**, *107*, 9514.
(98) Press, W. H.; Flannery, B. P.; Teukolsky, S. A.; Vetterling, W. T. *Numerical Recipes*; Cambridge University Press: Cambridge, 1986.